Estimating the Rate of Cessation of Magnetospheric Activity in AMPERE Field-Aligned Currents

Moretto, T.; Hesse, M.; Vennerstrøm, S.; Tenfjord, P.

Published in:
Geophysical Research Letters

Link to article, DOI:
10.1029/2018GL080631

Publication date:
2018

Document Version
Peer reviewed version

Estimating the Rate of Cessation of Magnetospheric Activity in AMPERE Field-Aligned Currents

T. Moretto[1,†], M. Hesse[1], S. Vennerstrøm[2], and P. Tenfjord[1]

[1]Birkeland Centre for Space Science, University of Bergen, Norway

[2]National Space Institute, DTU Space, Denmark

Corresponding author: first and last name (Therese.jorgensen@uib.no)

†Full name: Therese Moretto Jorgensen.

Key Points:

- Magnetospheric activity exhibits approximate exponential decay when solar wind driving is turned off (minimized).
- An average exponential time constant of 1.1 hours is measured in total hemispheric field-aligned current estimates.
- Longer decay time is observed in the summer compared to the winter hemisphere, consistent with expectations for ionospheric line-tying.

Abstract

The decay of magnetospheric activity when driving is turned off (to a minimum) was measured in total field-aligned current estimates from the AMPERE project. Events of distinct northward turnings of the IMF were identified, with prolonged periods of stable southward driving conditions followed by northward IMF conditions. All but four of 43 identified events exhibit a well-defined exponential decay in the total hemispheric field-aligned current following the northward turning. A superposed epoch analysis yields a generic decay constant of 0.9, corresponding to an e-folding time of 1.1hour. A statistical analysis of the ensemble of events also reveals a seasonal variation in the decay parameter with faster decay observed in the winter than in the summer hemisphere. This result can be understood in terms of stronger/weaker line-tying of the ionospheric foot-points of magnetospheric field-lines for higher/lower conductivity.

This article has been accepted for publication and undergone full peer review but has not been through the copyediting, typesetting, pagination and proofreading process which may lead to differences between this version and the Version of Record. Please cite this article as doi: 10.1029/2018GL080631

1 Introduction

The coupled magnetosphere-ionosphere system is a strongly driven system, for which the overall energy and circulation is largely determined by conditions of the solar wind and interplanetary magnetic field (IMF). In particular the strength and direction of the latter are crucial determining factors for magnetospheric convection and associated ionospheric currents and convection systems. Many studies over the last several decades have investigated the response in the magnetosphere and ionosphere convection and currents to changes in the IMF from a variety of ground-based and satellite observations (see, for example, Nishida, 1968; Friis-Christensen et al., 1985; Ridley et al., 1998; Murr and Hughes, 2001; Lu et al., 2002; Ruohoniemi et al., 2002; Fiori et al., 2012; Grocott and Milan, 2014; Dods et al., 2017; Snekvik et al., 2017; Anderson et al., 2018; McPherron et al., 2018, and references herein). These previous efforts have mostly focused on the processes and timescales involved in reacting to and setting up the new convection and current systems imposed by the change, particularly how activity is spun up following a southward turning of the IMF. In contrast, to our knowledge, only little information exists on the opposite process; how the activity (convection and associated currents) dies down following a northward turning and the consequent minimal driving conditions.

Few existing studies present results specifically for changes from southward to northward IMF conditions. Examinations of single individual events (e.g. Clauer and Friis-Christensen, 1988; Knipp et al., 1991; Hairston and Heelis, 1995) have reported typical reconfiguration times for ionospheric convection or current systems in the range of 20 to 40 minutes. Meanwhile, a statistical study by Ridley et al. (1998) found an average reconfiguration time of 13 minutes with no significant difference observed between north to south and south to north turnings. At the other end of the spectrum, Wygant et al. (1983), reported that introducing a weighted average of solar wind parameters over the preceding four hours, with a weighting function in the form of an exponential with a time scale of 3 hours, significantly improved agreement between observed polar cap potential drop and predictions based on hourly averaged solar wind parameters. They interpreted the existence of this extended time response in their results as the time constant for magnetospheric convection to «turn off» after previous periods of high reconnection rates. In a recent study, Hesse et al. (2017) also addressed the questions of what constitutes the most quiet state for the magnetosphere and how it is approached following a northward turning in the IMF that minimizes the driving. Utilizing global MHD modeling they observed an exponential decay with a decay time of about one hour in several integrated parameters related to different aspects of magnetospheric activity, including the total field-aligned current into and out of the ionosphere. Most recently, McPherron et al (2018) determined linear prediction filters in response to solar wind driving for total field-aligned currents on the dayside and nightside, respectively. They found response functions in both cases with total lengths of 3 hours but with different decay shapes, neither of which was seems to exhibit purely exponential decay.

The motivation of the work presented here is to provide new observational evidence for this decay rate. With the advent in 2010 of the Active Magnetosphere and Planetary Electrodynamics Response Experiment (AMPERE) project we now have available continuous global estimates of the field-aligned currents into and out of the high latitude ionosphere (Anderson et al., 2014). Field-aligned Birkeland currents play a fundamental role in magnetosphere-ionosphere coupling as the main means for conveying stresses within the system (e.g. Cowley, 2000). The AMPERE measurements, therefore, constitute an ideal new resource for assessing the level of the large-scale convection in the magnetosphere that we shall utilize for this purpose. Below we first describe the data sets that have been used,

followed by the results of a superposed epoch analysis and the results of a statistical analysis, and ending with a discussion and our conclusions.

2 Data and Event Selection

The OMNI dataset available from the GSFC/SPDF OMNIWeb interface at https://omniweb.gsfc.nasa.gov provides observations of solar wind plasma parameters and Interplanetary magnetic field (IMF) obtained by various satellites far upstream of the Earth magnetopause and propagated to the estimated location of the sub-solar bow shock. For this study we made use of the high-resolution (one-minute) measurements. Periods of steady driving interrupted by rapid shifts from southward to northward IMF conditions were identified in the IMF data by the following requirement: steady driving with southward IMF (IMF Bz < -2 nT) for at least 80 minutes followed by a fast (<20 minutes) northward turning and steady northward IMF (IMF Bz > 2 nT) for at least 80 minutes afterwards. Applying this criterion to the OMNI IMF data for the seven year period 2010-2016 yielded 48 events, which constitute the ensemble of candidate events that are available to examine how magnetospheric activity decays when driving is suddenly turned off (to a minimum).

Since January 2010, the AMPERE project has routinely obtained global estimates of the radial currents into and out of the high latitude ionosphere for both the southern and northern hemispheres (Anderson et al., 2014). Time series of integrated total upward and downward current estimates for each hemisphere are some of the standard products provided by the AMPERE project. Adopting the approach of earlier studies (Anderson et al, 2014, 2017, and 2018; Coxon et al, 2016), we use half of the sum of the absolute values of the upward and downward currents for each hemisphere as a measure of the total current. As explained in Anderson et al, 2014, the degree to which the upward and downward total hemispheric currents do not match is an indication of the uncertainty in these total current estimates. AMPERE total field aligned current estimates are available for 43 of the events identified in the OMNI IMF data. A listing of the events is provided in the supporting information. For the AMPERE measurements included in this study, the median difference between upward and downward total current estimates overall is 0.2MA for both the northern and southern hemispheres, which is consistent with values quoted in Anderson et al., 2017. Since the total current estimates are lower, on average, for the south (median value of 2.4MA across all measurements used in the study) than the north (median of 3.0MA), these differences correspond to median errors on the total current estimates of 6% and 10%, respectively, for the northern and southern hemispheres. The fact that the estimates, over all, for the southern hemisphere have lower values and higher errors than for the north is discussed, for example, in Coxon et al. (2016), Anderson et al. (2017), and Anderson et al. (2018). Possibly, this inter hemispheric difference is a result of the difference in offset between the magnetic and geographic poles or in the magnetic field strength at the two poles, both of which may affect the Birkeland currents through their effect, amongst others, on the ionospheric conductivity (e.g. Laundal et al., 2017). Specifically, the former introduces a larger difference between summer and winter conditions for the auroral oval in the north, as compared to the south, because a larger portion of the auroral oval is sunlit during summer in the north than in the south and a larger portion of the oval is in darkness during winter in the north than in the south. However, it also cannot be ruled out that the observed difference in the AMPERE measurements results, at least in part, from orbital differences of the satellites relative to the geomagnetic pole in the two hemispheres (Coxon et al., 2016). Finally, our ensemble of events has a small seasonal bias that may affect the amplitude averages obtained for the two hemispheres: 11 of the 39 events occur within 45 days of the June solstice and only 4 events within 45 days of the December solstice date.

Two example events are presented in Figure 1. A solstice event with very strong driving is shown on the left and a low activity level equinox event is on the right. For each event, the top panel displays the three components of the IMF from the OMNI database for a four hour interval centered on the time of the northward turning that identifies the event. The bottom panel for each event displays along the same timeline the AMPERE total current estimates (dotted lines) for the northern (red) and southern (blue) hemispheres together with exponential fits (full lines) to the decay in the currents observed after the northward turning: $I = I_0 \exp(-\lambda t_d)$. To allow for some time for the IMF change to propagate from the bow-shock to the magnetopause a short delay of 10 minutes is included in the exponential fit. Thus, the time t_d is the time in hours after the northward turning in the OMNI data minus the delay of 10 minutes. The parameters of the exponential fit (I_0 and λ) and the corresponding R-squared coefficient, which provides a measure of the goodness of the fit, are noted in each plot. Despite large differences in the overall amplitude level of the currents for the two events, they both exhibit profiles that are well matched by exponentials (R-squared >0.96 in all cases) and with fairly similar decay constants. The larger difference between the decay constants for the northern and southern hemispheres ($0.8h^{-1}$ and $1.7h^{-1}$, respectively) during solstice as well as the differences between either of those and the equinox values ($1.1h^{-1}$ and $1.0h^{-1}$) are illustrative of findings we shall document below.

Only three of the 43 events do not display a clear decay following the northward turning with resulting poor exponential fits (R-squared less than 0.3 for either one or both hemispheres). These events are a consequence of the simple event selection criteria used, which do not control for other driving parameters, such as IMF By or solar wind speed. The events were not included in the analyses presented in the following sections. One additional event was discarded because it displays an abnormal current profile with a strong peak following the northward turning, presumably caused by large IMF By variations, and a resulting decay constant that is an outlier in the distribution by more than 5 sigma. This leaves 39 events in the sample, only three of which exhibit an R-squared value for one, but not both, of the hemispheres of less than 0.7. All other events included in the study fit exponential decays with an R-squared value larger than 0.7 for both hemispheres. The median of the R-squared coefficient for the 39 events is 0.9 for both hemispheres.

3 Superposed Epoch Analysis

Organizing the 39 events around the northward turning of the IMF as shown in Figure 1, we carried out a superposed Epoch analysis of the decay of the currents in both hemispheres and also of the driving conditions for the events. The results for the IMF measurements are displayed in Figure 2.

In the top left panel are plotted the time lines (in a format similar to that used in Figure 1) for the GSM Z-component of the IMF for all events (grey curves) and overlaid (thick blue curve) is the median over all events at each time step (every 1 minute). The top right panel displays the same plot for the GSM Y-component of the IMF. On average, the events represent a change in IMF Bz from -5nT to +5nT, while displaying a slight preference for negative By (median of -1.2nT over all events) but with no discernible systematic change in By with respect to the northward turning from which the events have been identified. The median for the absolute magnitude of the IMF Bz component over the entire 7 year period (2010-2016) is 2.0nT and for the absolute magnitude of IMF By it is 2.7nT. The higher than average median value for IMF Bz both before and after the turning, presumably, is a result of requiring stable conditions for the component for an extended period of time. Similarly, we

find (not shown) slightly enhanced solar wind density for the events (median of 6.2cm^{-3} compared to 4.6cm^{-3} overall), whereas the solar wind speed for the events are nominal (median of 410km/s for the events and 394km/s overall).

The corresponding results for the total AMPERE field-aligned current estimates are displayed in the bottom panels of Figure 2. In the bottom left panel are plotted the total AMPERE field-aligned currents for all events for both hemispheres (grey curves) and overlaid (thick blue curve) is the median over all events at each time step (every 2 minutes), in which the characteristic exponential decay following the northward turning is observed just as for the single events of Figure 1. In order to get a robust measure for the overall decay rate, we normalized the current profiles for each event, and each hemisphere, with respect to the current measurement at 10 minutes past the northward turning. The resulting profiles are plotted in the bottom right panel (grey curves) and overlaid (thick blue curve) is again the median over all events. Also overlaid in this plot (magenta dotted curve) is the exponential fit to the decay of the median current following the northward turning in IMF plus a delay of 10 minutes like for the individual events of Figure 1. The parameters of the fit and the R-squared coefficient are noted on the figure. Notably, we find an astoundingly good fit to an exponential decay (R-squared coefficient of 0.99). The measured decay constant is 0.92h^{-1} corresponding to an exponential time constant, or e-folding, time of 1.1 hours.

4 Statistical Analysis

While the superposed epoch analysis described in the previous section presents a clear picture of the decay of the total current, it also reveals substantial variations in all of the parameters across the set of events. To gain further insight into the breadth of the results for the events and what might be the root-cause of it, we present the ensemble of events in more detail.

Exponential decay fitting as illustrated in Figure 1 was carried out for each event individually. The resulting distribution of fitting parameters is shown in Figure 3 for the entire ensemble of events. Parameter sets for each event (north and south estimates separately) are indicated by colored dots (grey, red, and blue, the distinction between which will be discussed later) with the current at the start of the decay, i.e. 10 minutes after the northward turning, plotted along the x-axis and the decay constant along the y-axis. Also marked in the plot (large, light grey dot and bars) are the median (and standard variation) over all data points of the fitting parameters: Med(I_0) = 4.4 (± 2.7) MA and Med(λ) = 0.89 (± 0.33)h^{-1}, which are in perfect agreement with the results from the superposed epoch analysis.

The scatter in the parameters is large but indicate no clear dependence of the decay constant on the amplitude of the current at the start of the decay (correlation coefficient 0.1, and 30% probability of no correlation). A multiple linear regression analysis (not shown) did reveal a few other potential dependencies for λ, including the amplitude of the change in IMF Bz (positive correlation) and the ratio of absolute values of Bz and By after the northward turning (negative correlation). However, most of these dependencies are all weak and only marginally significant. Given the relatively small sample size together with the large spread in λ values and large number of possible influencing variables this is not very surprising. One variable was found to have a significant impact on the decay, though, namely characterizing the events by season. Events occurring during local summer or winter (45 days on either side of the corresponding solstice date) are marked with red and blue colors, respectively, in Figure 3. A clear separation is observed, with summer events displaying, on average, lower values and winter events higher values for λ, corresponding to

longer and shorter decay times, respectively. The median (and standard variation) for the fitting parameters for the solstice events are: Med(I_0) = 5.2 (± 3.8) MA and Med(λ) = 0.75 (± 0.28)h^{-1} for the summer events and Med(I_0) = 3.6 (± 2.6) MA and Med(λ) = 1.1 (± 0.36)h^{-1} for the winter events. A standard student t-test (e.g. Welch, 1947) confirms that this separation with season is significant with better than 99.9% probability.

5 Discussion and Conclusion

The observation that magnetospheric activity undergo a characteristic exponential decay following a northward turning in the IMF confirms the earlier findings of Wygant et al. (1983). With a larger number of events and a more direct measure we have obtained a more accurate estimate for the decay time than the 2-3 hours they deduced: we found a decay constant λ = 0.9 (± 0.3) h^{-1} which corresponds to a time constant of 0.8-1.7 hours. This result fully confirms the prediction of 0.93 hours for the time constant obtained by Hesse et al. (2017) based on global MHD modeling. Further, in agreement with our finding that the decay rate does not depend on the level of activity before the northward turning, they also found no change in the decay rate when varying the initial driving conditions. A possible physical explanation for the exponential decay follows from considering what needs to happen for the convection in the magnetosphere to slow down, or stop, namely the unwinding of the field-aligned current carrying fluxtubes in the coupled magnetosphere-ionosphere system. The exponential time constant of roughly one hour measured here and the 3-hours length of the response filters reported by McPherron et al. (2018), suggest good overall consistency between the results from these different analysis methods applied to the same AMPERE dataset. However, while the results here indicate exponential decay, the McPherron et al. (2008) analysis seemingly results in functional decay shapes that are not purely exponential. This discrepancy warrants further investigation but is beyond the scope of this report.

Our statistical analysis of the ensemble of events also revealed a seasonal variation in the decay parameter with faster decay observed in the winter than in the summer hemisphere. Since no clear dependence on the amplitude of the current was found for the decay parameter, we conclude that the seasonal variation in ionospheric conductivity independently affect both the amplitude of the current and the decay parameter. Motion of the plasma in the ionosphere is imposed by convection in the magnetosphere through the JxB force. In response, the ionosphere with higher conductivity (summer conditions) will have a higher resistance to motion thus necessitating a larger current to establish the appropriate magnetosphere-ionosphere coupling. Oppositely, an ionosphere with low conductivity will not strongly oppose motion imposed by the magnetosphere and comparatively little current is needed to establish the coupling. These effects are well documented (e.g Ridley, 2007; Coxon et al, 2016). At the same time, stronger/weaker line-tying in the higher/lower conductivity ionosphere may also explain the longer/shorter decay time for magnetospheric activity. With low conductivity in the ionosphere and corresponding weaker line-tying of magnetospheric field lines the unwinding of current-carrying fluxtubes and associated changes in magnetospheric convection that need to happen to reach the new quiet state can be more easily and quickly accomplished (e.g. Coroniti and Kennel, 1973). The opposite is true for the high conductivity case where stronger line-tying makes changes in convection take longer to get established.

Acknowledgments

Total current estimates from the Active Magnetosphere and Planetary Electrodynamics Response Experiment (AMPERE) project, PI Brian Anderson, JHU/APL,

were downloaded from the project website at http://ampere.jhuapl.edu. We are grateful to the AMPERE team and the AMPERE Science Center for providing the Iridium- derived data products. We acknowledge use of NASA/GSFC's Space Physics Data Facility's CDAWeb service and high-resolution (1 minute) OMNI data to provide solar wind and IMF parameters propagated to the sub-solar bowshock. The data was retrieved through the OMNIWeb interface at https://omniweb.gsfc.nasa.gov. This research was supported by the Research Council of Norway/CoE under contract 223252/F50.

References

Anderson, B. J., H. Korth, C. L. Waters, D. L. Green, V. G. Merkin, R. J. Barnes, and L. P. Dyrud (2014), Development of large-scale Birkeland currents determined from the Active Magnetosphere and Planetary Electrodynamics Response Experiment, *Geophys. Res. Lett.*, 41, 3017–3025, doi: 10.1002/2014GL059941

Anderson, B. J., H. Korth, D. T. Welling, V. G. Merkin, M. J. Wiltberger, J. Raeder, R. J. Barnes, C. L. Waters, A. A. Pulkkinen, and L. Rastaetter (2017), Comparison of predictive estimates of high-latitude electrodynamics with observations of global-scale Birkeland currents, *Space Weather*, 15, 352–373, doi: 10.1002/2016SW001529

Anderson, B. J., Olson, C. N., Korth, H., Barnes, R. J., Waters, C. L., & Vines, S. K. (2018). Temporal and spatial development of global Birkeland currents, *J. Geophys. Res. Space Physics*, 123, doi.org/10.1029/2018JA025254

Clauer, C. R. & E. Friis-Christensen (1988), High-latitude dayside electric fields and currents during strong northward interplanetary magnetic field: Observations and model simulation, *J. Geophys. Res.*, 93(A4), 2749–2757, doi: 10.1029/JA093iA04p02749

Coroniti, F. V. & C. F. Kennel (1973), Can the ionosphere regulate magnetospheric convection?, *J. Geophys. Res.*, 78(16), 2837–2851, doi: 10.1029/JA078i016p02837

Cowley, S. W. H. (2000), Magnetosphere-ionosphere interactions: A tutorial review, in Magnetospheric Current Systems, *Geophys. Monogr. Ser.*, vol. 118, edited by S. Ohtani et al., pp. 91–106, AGU, Washington, D. C.

Coxon, J. C., S. E. Milan, J. A. Carter, L. B. N. Clausen, B. J. Anderson, and H. Korth (2016), Seasonal and diurnal variations in AMPERE observations of the Birkeland currents compared to modeled results, *J. Geophys. Res. Space Physics*, 121, 4027–4040, doi:10.1002/2015JA022050

Dods, J., S. C. Chapman, and J. W. Gjerloev (2017), Characterizing the ionospheric current pattern response to southward and northward IMF turnings with dynamical SuperMAG correlation networks, *J. Geophys. Res. Space Physics*, 122, 1883–1902, doi:10.1002/2016JA023686

Fiori, R. A. D., D. H. Boteler, and A. V. Koustov (2012), Response of ionospheric convection to sharp southward IMF turnings inferred from magnetometer and radar data, *J. Geophys. Res.*, 117, A09302, doi: 10.1029/2012JA017755

Friis-Christensen, E., Y. Kamide, A. D. Richmond, and S. Matsushita (1985), Interplanetary magnetic field control of high-latitude electric fields and currents determined from Greenland Magnetometer Data, *J. Geophys. Res.*, 90(A2), 1325–1338, doi: 10.1029/JA090iA02p01325

Grocott, A. & S. E. Milan (2014), The influence of IMF clock angle timescales on the morphology of ionospheric convection, *J. Geophys. Res. Space Physics*, 119, 5861–5876, doi: 10.1002/2014JA020136

Hairston, M. R., and R. A. Heelis (1995), Response time of the polar convection pattern to changes in the north-south direction of the IMF, *Geophys. Res. Lett.*, 22, 631, doi: 10.1029/94GL03385

Hesse, M., T. Moretto, M. Kuznetsova, P. Tenfjord, C. Norgren, N. Østgaard, E. Friis-Christensen, and H. Opgenoorth (2017), Does the Magnetosphere go to Sleep?, *AGU Fall Meeting 2017*, abstract #SM13A-2353, available from: adsabs.harvard.edu/abs/2017AGUFMSM13A2353H

Knipp, D. J., A. D. Richmond, B. Emery, N. U. Crooker, O. de la Beaujardiere, D. Evans, and H. Kroehl (1991), Ionospheric convection response to changing IMF direction, *Geophys. Res. Lett.*, 18(4), 721–724, doi: 10.1029/90GL02592

Laundal, K.M., I. Cnossen, S.E. Milan, S. E. Haaland, J. Coxon, N. M. Pedatella, M. Förster, J. P. Reistad (2017), North–South Asymmetries in Earth's Magnetic Field: Effects on High-Latitude Geospace, *Space Sci Rev* 206: 225., doi: 10.1007/s11214-016-0273-0

Lu, G., T. E. Holzer, D. Lummerzheim, J. M. Ruohoniemi, P. Stauning, O. Troshichev, P. T. Newell, M. Brittnacher, and G. Parks (2002), Ionospheric response to the interplanetary magnetic field southward turning: Fast onset and slow reconfiguration, *J. Geophys. Res.*, 107(A8), doi: 10.1029/2001JA000324

McPherron, R. L., B. J. Anderson, and X. Chu (2018), Relation of field-aligned currents measured by the network of Iridium® spacecraft to solar wind and substorms, *Geophys. Res. Lett.*, 45, 2151–2158, doi: 10.1002/2017GL076741

Murr, D. L. & W. J. Hughes (2001), Reconfiguration timescales of ionospheric convection, *Geophys. Res. Lett.*, 28(11), 2145–2148, doi: 10.1029/2000GL012765

Nishida, A. (1968), Coherence of geomagnetic DP 2 fluctuations with interplanetary magnetic variations, *J. Geophys. Res.*, 73(17), 5549–5559, doi: 10.1029/JA073i017p05549

Ridley, A. J., G. Lu, C. R. Clauer, and V. O. Papitashvili (1998), A statistical study of the ionospheric convection response to changing interplanetary magnetic field conditions using the assimilative mapping of ionospheric electrodynamics technique, *J. Geophys. Res.*, 103(A3), 4023–4039, doi: 10.1029/97JA03328

Ridley, A. J. (2007), Effects of seasonal changes in the ionospheric conductances on magnetospheric field-aligned currents, *Geophys. Res. Lett.*, 34, L05101, doi: 10.1029/2006GL028444

Ruohoniemi, J. M., S. Shepherd, and R. Greenwald (2002), The response of the high-latitude ionosphere to IMF variations, *J. Atmos. Sol. Terr. Phys.*, 64, 159–171, doi: 10.1016/S1364-6826(01)00081-5

Snekvik, K., N. Østgaard, P. Tenfjord, J. P. Reistad, K. M. Laundal, S. E. Milan, and S. E. Haaland (2017), Dayside and nightside magnetic field responses at 780 km altitude to dayside reconnection, *J. Geophys. Res. Space Physics*, 122, 1670–1689, doi: 10.1002/2016JA023177

Welch, B. L. (1947), The generalization of "Student's" problem when several different population variances are involved", *Biometrika*, **34** (1–2): 28–35, doi:10.1093/biomet/34.1-2.28

Wygant, J. R., R. B. Torbert, and F. S. Mozer (1983), Comparison of S3-3 polar cap potential drops with the interplanetary magnetic field and models of magnetopause reconnection, *J. Geophys. Res.*, 88(A7), 5727–5735, doi: 10.1029/JA088iA07p05727

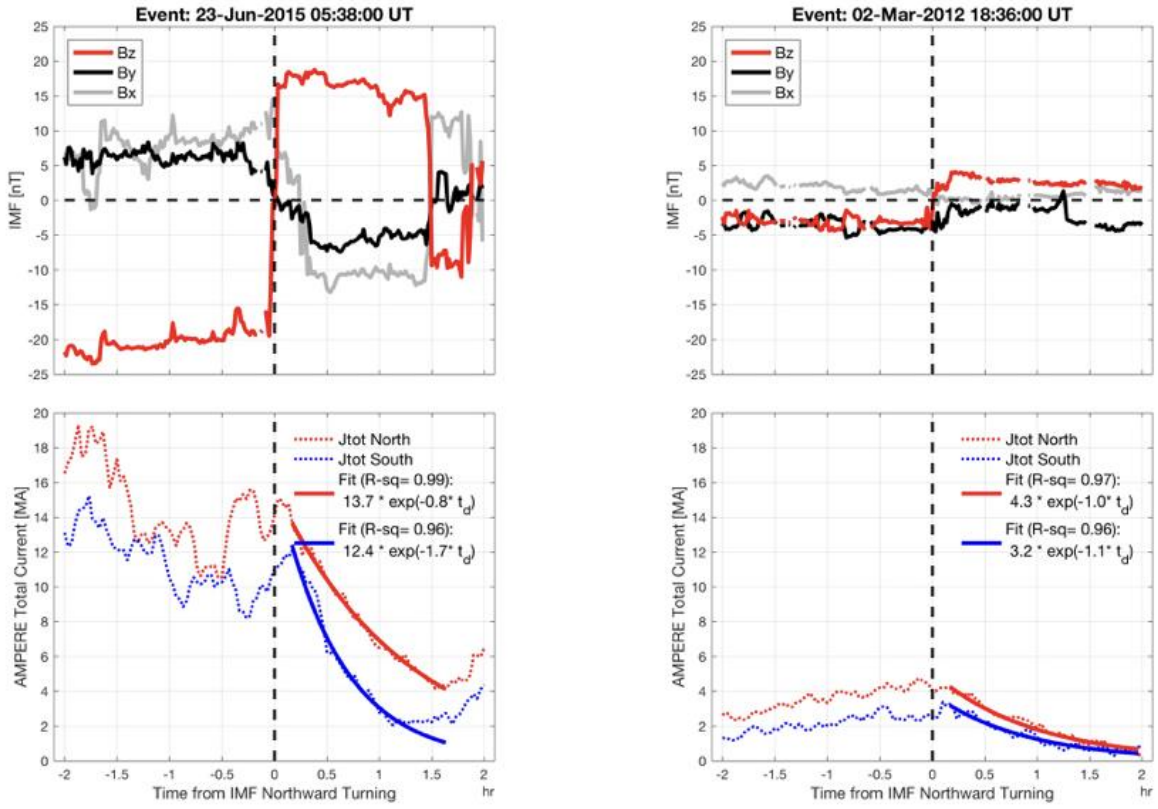

Figure 1. IMF (top panels) and total current estimates (bottom panels) for two northward turning example events.

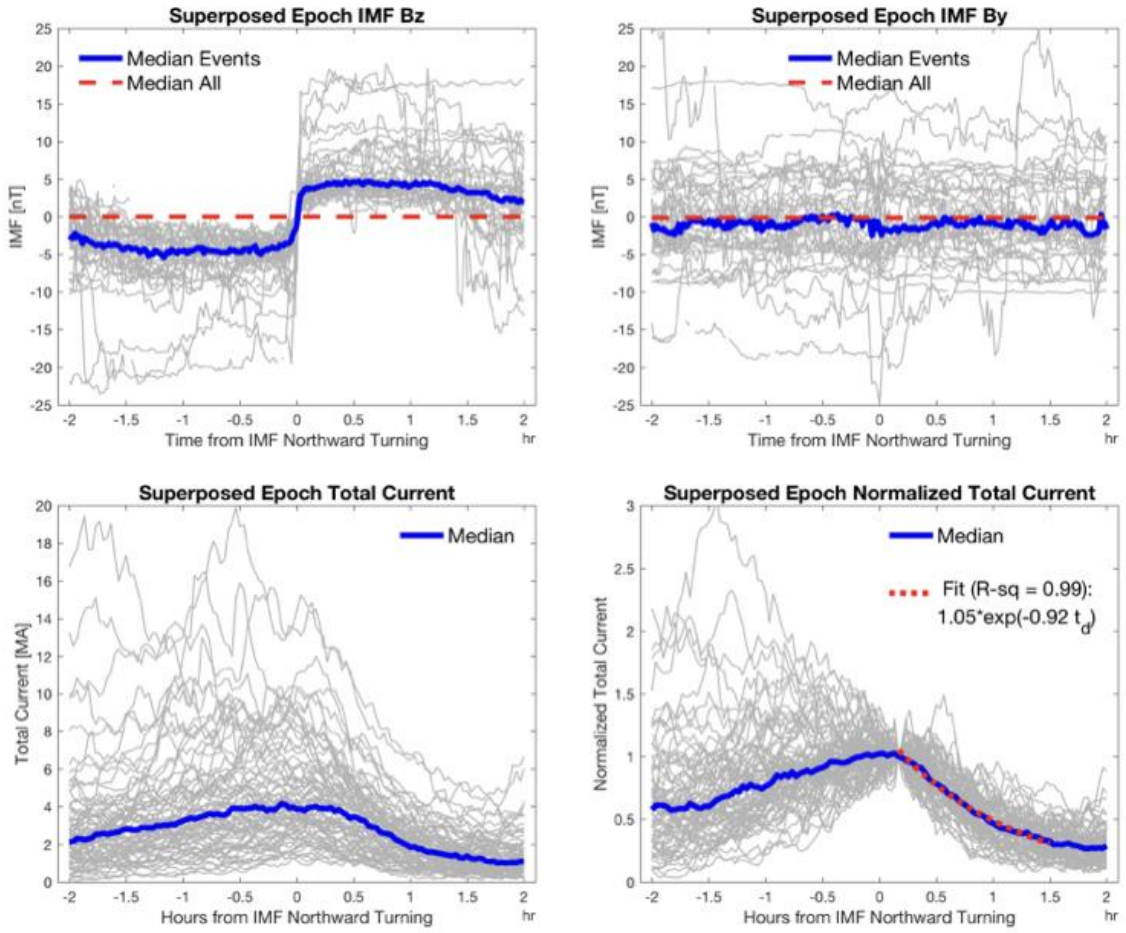

Figure 2. Superposed epoch plots of IMF Bz (top left), IMF By (top right), total hemispheric field-aligned current (bottom left), and normalized total current (bottom right).

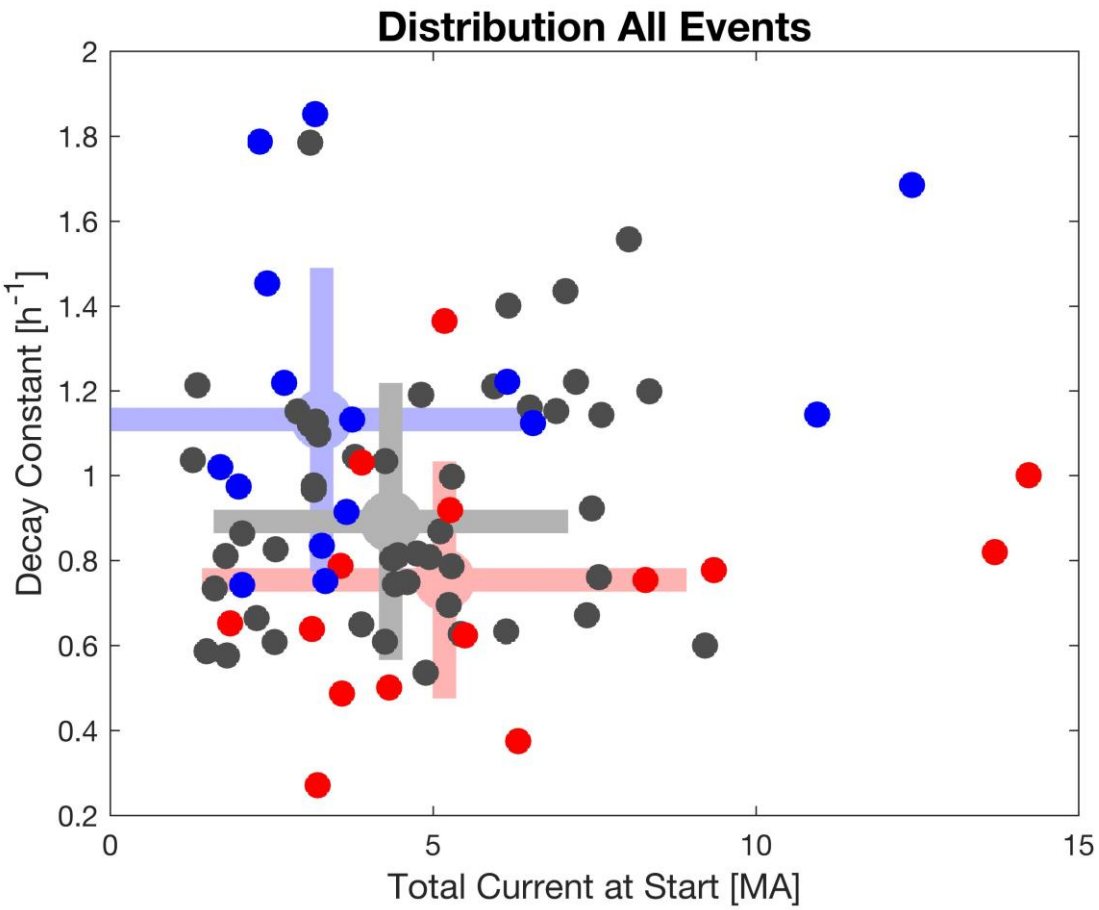

Figure 3. Scatter plot of fitting parameters for the entire ensemble of events and for the northern and southern hemispheres individually. The large, light grey dot and bars indicate the median values and standard deviations for the fitting parameters over the entire dataset. Marked in red are the events around the June solstice and in blue the events around the December solstice with corresponding medians and standard variations (large dots and bars in light red and blue), while the dark grey dots represent events that occur around the equinoxes.